AARHUS UNIVERSITY

quanTEEM
ERASMUS MUNDUS MASTER
QUANTUM TECHNOLOGIES
AND ENGINEERING

Reconfigurable SHG in Si_3N_4 Microrings via Self-Injection Locking and All-Optical Poling: A Design Study

Photonic Integrated Circuits

December 11, 2025

B. E. Castiblanco[1]

MSc Physics – Erasmus Mundus Master in Quantum Technologies and Engineering
QuanTEEM

Department of Physics and Astronomy, Aarhus University

[1] au786622@uni.au.dk

Abstract

This report presents a design study of second-harmonic generation (SHG) in silicon nitride (Si_3N_4) microring resonators by leveraging all-optical poling (AOP) and self-injection locking (SIL) to induce an effective second-order nonlinearity $\chi^{(2)}_{\text{eff}}$. The study aimed to evaluate the feasibility of quasi-phase-matched SHG in dispersion-engineered, CMOS-compatible Si_3N_4 waveguides. Using EMode-based simulations of straight waveguides—justified by the large microring radius ($R = 900\,\mu\text{m}$)—the effective refractive indices were extracted, computing the phase mismatch Δk and QPM period Λ_{QPM} across the C- and L- band. AOP dynamics were modeled using a photogalvanic rate equation, leading to a numerical fit of $\chi^{(2)}_{\text{eff}}(x)$ as a third-order polynomial in the waveguide width x, with the maximum $\chi^{(2)}_{\text{eff}} = 0.516$ pm/V occurring at $x = 900$ nm. This result aligned with the experimental findings in the literature and confirmed the maturity of the Si_3N_4 platform, despite being nearly two orders of magnitude lower than values typical of thin-film lithium niobate (TFLN). Simulations of SHG performance, incorporating the mismatch factor and cavity parameters, demonstrated enhanced efficiency under QPM but highlighted limitations in output power. These results underscored the potential of reconfigurable SHG in Si_3N_4 and provided a comprehensive modeling framework for guiding future experimental implementations.

Contents

1 Introduction

Nonlinear integrated photonics in silicon nitride (SiN) waveguides and resonators has attracted significant attention due to the wide transparency window (from visible to mid-IR), low propagation loss, moderate refractive index contrast, and CMOS compatibility of SiN platforms [5, 3]. While SiN is intrinsically centro-symmetric and thus lacks a bulk second-order susceptibility $\chi^{(2)}$, effective $\chi^{(2)}$ responses can be engineered via surface symmetry breaking, strain, or more recently via all-optical poling (AOP) based on the coherent photogalvanic effect [2]. In AOP, simultaneous excitation of a waveguide or resonator at the fundamental harmonic (FH) and second harmonic (SH) frequencies leads to a spatially modulated space-charge field, which in turn induces a quasi-phase-matching (QPM) $\chi^{(2)}$ grating through an effective third-order process, also known as *Electric-Field-Induced Second Harmonic Generation (EFISH)* [1].

In parallel, self-injection locking (SIL) of semiconductor lasers to high-Q microresonators allows large reductions in laser linewidth and frequency stabilization without electronic feedback.[2] Combining SIL, AOP, and second-harmonic generation (SHG) in SiN microrings offers a powerful route to compact, integrated visible-frequency sources and frequency combs.

Based on the above findings in scientific literature, the aim of this design study is to carry out straight-waveguide mode simulations of SiN/SiO_2 strucutres, by using `EMode Photonix` and obtaining the effective propagation constants and dispersion in order to: (i) compute the phase mismatch $\Delta k(\lambda)$ and QPM period relevant for SHG between FH and SH modes; (ii) embed these quantities into models of AOP and SHG in a doubly resonant microring; (iii) and finally explore numerically how quasi-phase matching via AOP modifies SHG conversion efficiency as a function of input power.

All the codes made, and the data and graphs obtained from the simulations, as well as a *complementary document* with a detailed extension of the theoretical framework implemented, can be consulted in the following `GitHub` repository:

2 Methodology

2.1 Waveguide Design and Platform

This design study explores SHG in a Si_3N_4 platform using AOP-induced $\chi^{(2)}$ nonlinearity. The choice for using a straight waveguide geometry is based on the large radius ($R \sim 900\,\mu$m) of equivalent ring resonators used in similar QPM-SHG demonstrations [2]. For example, ring radii in the range of hundreds of microns imply a weak curvature, justifying the straight approximation when evaluating phase-matching conditions and nonlinear coupling. This approximation significantly simplifies numerical mode solving and QPM period estimation.

Furthermore, the waveguide is fully cladded in silica (SiO_2), rather than leaving an air top cladding. This configuration not only ensures CMOS compatibility and mechanical robustness but also leads to enhanced core confinement. The confinement factor increases as the high-index contrast between Si_3N_4 and SiO_2 more effectively isolates the guided mode within the waveguide. This enhanced confinement directly improves overlap between the FH and SH modes, impacting the effective nonlinear coefficient.

A rectangular waveguide geometry is chosen over more complex rib or trapezoidal structures for the following reasons: (i) its compatibility with existing fabrication flows [5], (ii) predictable and reproducible dispersion characteristics, and (iii) the ease of mode solver convergence. The geometry is parametrized by varying width from 600 to 1800 nm, in steps of 100 nm, while keeping the height fixed at 600 nm, consistent with experimental precedents in AOP-enhanced SHG in Si_3N_4 [3, 7]. The wavelength sweep from 1520 nm to 1595 nm in 5 nm steps was selected to span the full C-band, which is compatible with standard telecom-grade lasers and detectors [5]. This resolution balances computational efficiency with sufficient spectral granularity to resolve meaningful changes in modal dispersion and phase-mismatch [8]. Moreover, this range overlaps with recent experimental SHG demonstrations in SiN resonators [2], enabling direct performance comparisons.

2.2 Theoretical Model and Simulation Flow

For a full detailed explanation of the theoretical model, specially regarding the SIL process and AOP Growth, consult the *complementary document* at the `GitHub` repository of the design study project.

The simulation methodology proceeded as follows:

1. Mode solving is conducted using `EMode`, extracting effective refractive indices, mode areas, and confinement factors at both 1550 nm (FH) and 775 nm (SH).

2. From the simulated effective indices, the phase mismatch Δk is computed as:

$$\Delta k = 2k_{\mathrm{FH}} - k_{\mathrm{SH}} = 2\frac{2\pi n_{\mathrm{FH}}}{\lambda_{\mathrm{FH}}} - \frac{2\pi n_{\mathrm{SH}}}{\lambda_{\mathrm{SH}}}, \tag{1}$$

   where n_{FH} and n_{SH} are the effective indices.

3. The QPM period is determined via $\Lambda_{\mathrm{QPM}} = 2\pi/\Delta k$.

4. A mismatch factor based on the $\mathrm{sinc}^2(\Delta k L/2)$ response is computed, capturing the efficiency reduction due to imperfect phasematching.

5. Hotspot analysis is conducted through thermal sensitivity and resonance tracking to identify optimal detuning tolerances for FH and SH. This is based on minimum $|DET|$ values across a ΔT sweep.

6. The AOP inscription is modeled through a coupled nonlinear rate-equation framework [8], assuming photoinduced gratings via coherent photogalvanic effect.

7. Effective $\chi^{(2)}$ growth is tracked and fitted as a function of waveguide width.

8. Finally, SHG output power and its steady-state limit are evaluated for both the QPM and natural-mismatch scenarios.

The full workflow is summarized in Figures in 1, illustrating the integrated waveguide structure and AOP inscription concept.

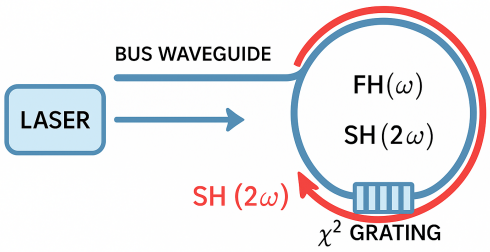

(a) Schematic of laser coupling to $\chi^{(2)}$ waveguide.

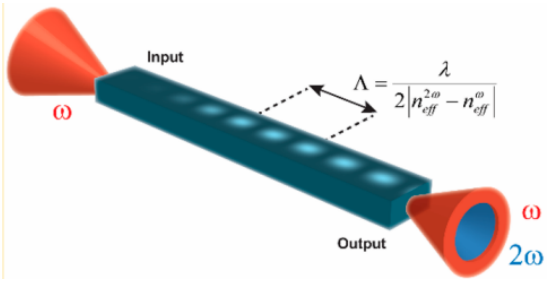

(b) Concept of QPM $\chi^{(2)}$ grating via AOP. Taken from [6].

Figure 1: Experimental and conceptual schematics used to frame the methodology.

3 Results and Discussion

3.1 Mode and Dispersion simulations

Figure 2 shows the $|E_x|^2$ field distribution for the FH case ($\lambda = 1595.0\,\mathrm{nm}$) and the SH ($\lambda = 797.5\,\mathrm{nm}$), with a core width of $x = 900\mathrm{nm}$. $|E_x|^2$ was chosen over E_x to better reflect energy localization and effective modal overlap, which directly influences nonlinear conversion efficiency.

3.2 Phase-Matching and Mismatch Analysis

Using the simulated effective indices across the sweep in wavelenght (1520 - 1600 nm), it was computed Δk and Λ_{QPM} for all widths. These quantities are shown in Figure 3. Δk decreases monotonically with wavelength, implying an increasing QPM period Λ as shown in Figure 3. This

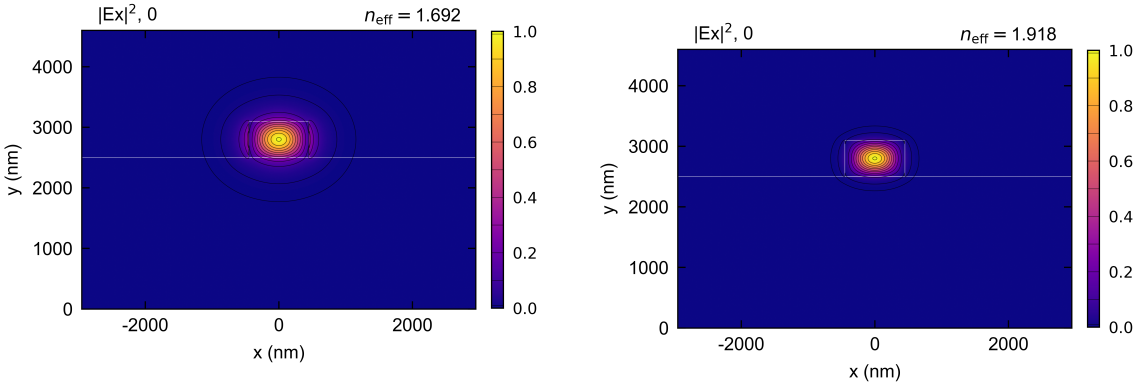

(a) Fundamental Harmonic mode (FH) at $\lambda = 1595.0\,\text{nm}$.

(b) Second Harmonic mode (SH) at $\lambda = 797.5\,\text{nm}$.

Figure 2: Simulated $|E_x|^2$ distribution at FH and SH. High core confinement supports enhanced mode overlap.

trend is consistent with the dispersion properties of SiN waveguides, where SH modes exhibit tighter confinement. Importantly, the extracted QPM values (2.15 µm–2.35 µm) lie well within the achievable range of AOP-based gratings [3, 7]. This validates the feasibility of QPM-assisted SHG in dispersion-engineered SiN microrings.

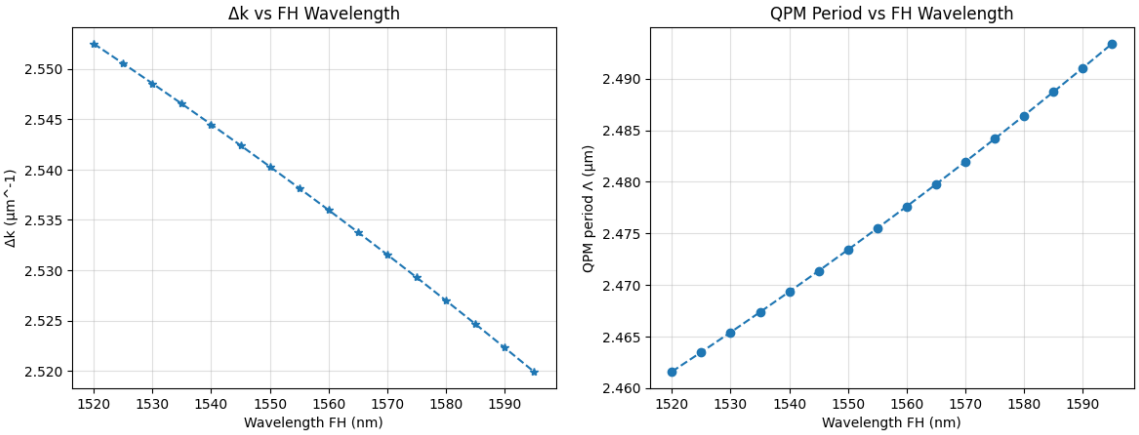

(a) Δk vs wavelength for the FH mode.

(b) Λ_{QPM} vs wavelength for the FH mode.

Figure 3: Phase-matching quantities extracted from the simulated modes by the sweep in wavelength (1520-1600 nm).

3.3 Double Resonance Hotspots and Minimum Detuning

Double resonance conditions were mapped by scanning detunings across thermal variations. Figure 4a shows clear hotspot distributions. Corresponding minimum detuning plots are included in Figure 4b. These graphs provide a map which serve to indicate where the chip temperature can be tuned, yielding the ring to be resonant simultaneously at the FH and SH modes. This is needed in order to have an efficient SHG. By looking at graph in Figure 4b, it is spotted that minimum detunnings are of the order of 10 pm, resolution that was used to get the hotspots in

Figure 4a.

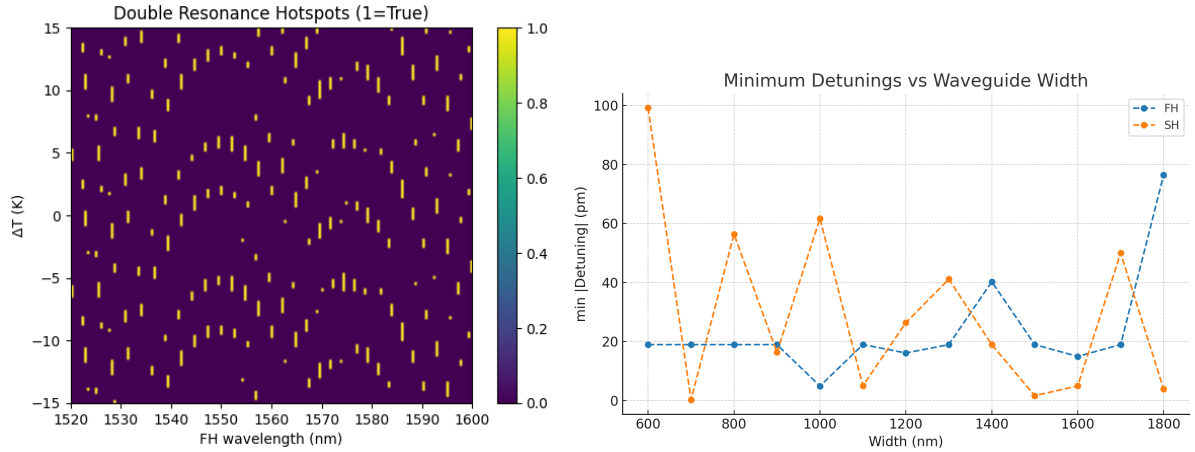

(a) Hotspot map vs T and FH.

(b) Minimum detunings for FH and SH.

Figure 4: Detuning resonance behavior.

3.4 AOP Dynamics and $\chi^{(2)}$ Extraction

The SIL mechanism stabilizes the FH resonance, ensuring that the AOP inscription remains aligned during exposure. This is modeled via standard rate equations (for more details consult the `GitHub` repository), and depends strongly on the effective area of the FH mode. The mode at width 900 nm was found to be the one that maximizes the confinement factor (76,2%) and minimizes the effective area ($0,846\,\mu m^2$) at the same time. The AOP-induced $\chi^{(2)}$ builds up as a function of exposure time (Fig. 5a).

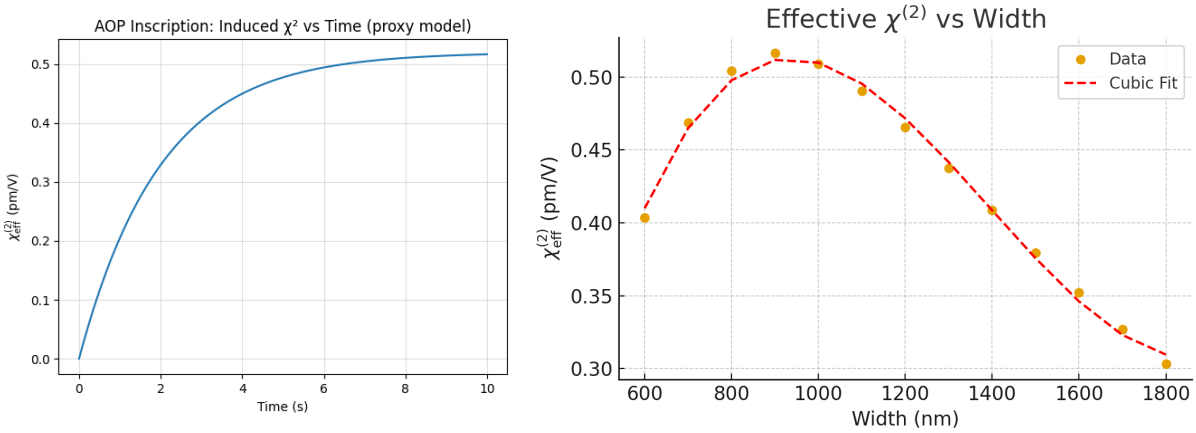

(a) $\chi^{(2)}$ vs inscription time.

(b) Effective $\chi^{(2)}$ vs width (fit included).

Figure 5: Photoinduced $\chi^{(2)}$ characteristics and fit.

A **key finding** of this design study is the dependency of the effective $\chi^{(2)}$ on the waveguide width. Figure 5b shows that $\chi^{(2)}_{\text{eff}}$ peaks at thw width of 900 nm with a maximum of 0.516 pm/V. This observation is consistent with optimal core confinement overlap and minimized phase mismatch. A polynomial interpolation was used to model this behavior, yielding to a third-order

fit:

$$\chi^{(2)}_{\text{eff}}(x) = \left(5.30 \times 10^{-10} \ \frac{\text{pm}}{\text{V} \cdot \text{nm}^3}\right) x^3 - \left(2.22 \times 10^{-6} \ \frac{\text{pm}}{\text{V} \cdot \text{nm}^2}\right) x^2 + \left(2.76 \times 10^{-3} \ \frac{\text{pm}}{\text{V} \cdot \text{nm}}\right) x - 0.562 \ \frac{\text{pm}}{\text{V}} \quad (2)$$

With x the waveguide width in nm, and a Pearson coefficient $R^2 = 0.995$.

This result aligns with values reported by Clementi et al. [2], who demonstrated $\chi^{(2)} \approx 0.54$ pm/V in a pretty much identical configuration. Although much lower than Thin-Films-Lithium-Niobate (TFLN) platforms (where $\chi^{(2)} \sim 54$ pm/V), the CMOS compatibility and yield of SiN across the photonics industry makes it an attractive platform for scalable nonlinear optics [5, 3].

3.5 SHG Performance

Figure 6 presents the simulated SHG output power. Despite low absolute SH output power ($\sim 4.7 \times 10^{-39}$ mW) after $\sim 100\,\mu$s, the trends confirm that QPM and AOP $\chi^{(2)}$ grating enables enhancement over natural Δk. This emphasizes the critical role of engineered $\chi^{(2)}$ and phase matching. The maximum steady-state SHG output power is around 3.6×10^{-37} mW. This is low, indicating either the nonlinear conversion length is insufficient, the mode overlap is suboptimal, or input intensities are too low. Improvements could be achieved by higher-Q resonators, tighter mode overlaps, or increased interaction length [4].

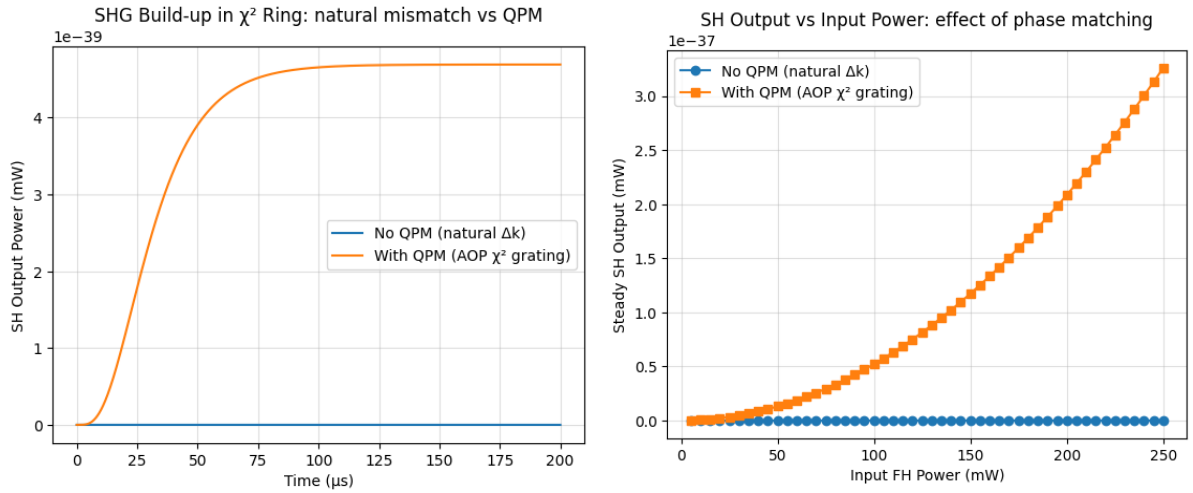

(a) SHG transient power.

(b) Steady SHG output vs input.

Figure 6: SHG performance curves with and without QPM grating.

4 Conclusion

This project explored second-harmonic generation (SHG) in silicon nitride (Si_3N_4) microrings enabled by self-injection locking (SIL) and all-optical poling (AOP). By leveraging eigenmode simulations of rectangular straight waveguides, the effective modal parameters were extracted, finding phase-matching conditions relevant to microring geometries. A full sweep in wavelength (1520–1595 nm) allowed precise evaluation of phase mismatch Δk, quasi-phase-matching (QPM)

periods, and mismatch suppression factors, forming the foundation for SHG modeling under realistic dispersion conditions.

Also, a geometry sweep was carried out, varying the waveguide core from 600 to 1800 nm, finding that the width $x = 900$ nm maximizes the photoinduced effective nonlinearity, yielding $\chi^{(2)}_{\text{eff}} \approx 0.516$ pm/V, consistent with the best values reported in state-of-the-art experiments. A third-order polynomial fit captured the dependence of $\chi^{(2)}_{\text{eff}}$ on waveguide width, enabling predictive design across geometries. Despite this moderate nonlinearity, the results underscored the potential of Si_3N_4 as a CMOS-compatible platform for reconfigurable nonlinear photonics, with added value due to its stability and mature fabrication ecosystem.

Finally, nonlinear time-domain simulations demonstrated the importance of QPM and resonance alignment on SHG efficiency, showing that under ideal QPM conditions, second-harmonic output powers reached up to $\sim 4.7 \times 10^{-39}$ mW after $\sim 100\,\mu$s, with a maximum steady-state SHG output power around 3.6×10^{-37} mW, in comparison with null SHG outpower when considering only the natural Δk. These results, although minimal, highlight the critical role of poling and double resonance. Future work may include experimental validation of the optimal width, design of advanced grating schemes for improved AOP performance, and integration with pump lasers and active control for fully monolithic SHG sources.

References

[1] Robert W Boyd, Alexander L Gaeta, and Enno Giese. "Nonlinear optics". In: *Springer Handbook of Atomic, Molecular, and Optical Physics*. Springer, 2008, pp. 1097–1110.

[2] Marco Clementi et al. "Correction: A chip-scale second-harmonic source via self-injection-locked all-optical poling". In: *Light, Science & Applications* 14 (2025), p. 366.

[3] Jianqi Hu et al. "Photo-induced cascaded harmonic and comb generation in silicon nitride microresonators". In: *Science Advances* 8.50 (2022), eadd8252.

[4] Nikita M Kondratiev et al. "Recent advances in laser self-injection locking to high-Q microresonators". In: *Frontiers of Physics* 18.2 (2023), p. 21305.

[5] David J Moss et al. "New CMOS-compatible platforms based on silicon nitride and Hydex for nonlinear optics". In: *Nature photonics* 7.8 (2013), pp. 597–607.

[6] Edgars Nitiss et al. "Formation rules and dynamics of photoinduced χ (2) gratings in silicon nitride waveguides". In: *ACS photonics* 7.1 (2019), pp. 147–153.

[7] Edgars Nitiss et al. "Optically reconfigurable quasi-phase-matching in silicon nitride microresonators". In: *Nature Photonics* 16.2 (2022), pp. 134–141.

[8] Yun Zhao et al. "Theory of χ (2)-microresonator-based frequency conversion". In: *Optics Letters* 46.21 (2021), pp. 5393–5396.